LA-UR- 09-04173

Approved for public release; distribution is unlimited.

Title:	Pseudo One-Dimensional Analysis of Polymer Electrolyte Fuel Cell Cold-Start
Author(s):	Yun Wang (not LANL) Jeff Mishlera (not LANL) Partha P. Mukherjee Rangachary Mukundan Rodney L. Borup
Intended for:	216th ECS Meeting Vienna, Austria October 4-9, 2009

Form 836 (7/06)

Pseudo One-Dimensional Analysis of Polymer Electrolyte Fuel Cell Cold-Start

Yun Wang[a], Jeff Mishler[a], Partha P. Mukherjee[b], Rangachary Mukundan[b], and Rodney L. Borup[b]

[a]Renewable Energy Resources Lab, The University of California, Irvine, California, 92697-3975, USA
[b]Los Alamos National Laboratory, Los Alamos, NM, 87545, USA

This paper investigates the electrochemical kinetics, oxygen transport, and solid water formation in polymer electrolyte fuel cell (PEFC) during cold start. Following [Y. Wang, J. Electrochem. Soc., 154 (2007) B1041-B1048.], we develop a pseudo one-dimensional analysis, which enables the evaluation of the impact of ice volume fraction and temperature variations on cell performance during cold-start. The oxygen profile, starvation ice volume fraction, and relevant overpotentials are obtained. This study is valuable for studying the characteristics of PEFC cold-start.

INTRODUCTION

The polymer electrolyte fuel cell (PEFC) has been widely regarded as a potential power source for portable and automotive applications. PEFCs must have the ability to survive and start up from sub-freezing temperatures, also called cold start, if they are to be successfully deployed in automobiles. Under freezing environmental conditions, produced water within the membrane electrode assembly (MEA) of a fuel cell will freeze to form ice, which reduces cell performance and even shuts down fuel cell operation.

Cold-start is essentially a transient phenomenon. Currently, the majority of the efforts are focused on the steady-state characteristics of PEFCs. There is a lack of thorough investigation on the dynamic behavior, though the importance of dynamic characteristics is obvious for automobile and portable applications of fuel cells which are frequently subjected to fast load variations. While the characteristics of PEFC dynamics have been studied by several groups [1-11], research on PEFC cold start is relatively new [12-20]. Hishinuma et al. [12], Wilson et al. [13], McDonald el al.[14] and Cho et al.[15] conducted early studies on cold start. Hishinuma et al.[12] investigated cold-start down to ~-25°C and found waste heat generated by fuel cell might be sufficient to increase the PEFC temperature to 0 °C. Wilson et al. [13] investigated the impact of the freeze/thaw cycles on the electrode performance and concluded that freezing may not be detrimental to the integrity of the catalyst layer and membrane assembly. McDonald el al. [14] also conducted experiments to investigate the physical change in the electrolyte membrane due to freeze/thaw cycling. Cho et al. [15] carried out a study on cell degradation related to the thermal cycle and concluded that water freezing may be a source of cell degradation. Recently, Oszcipok et al. [16] examined the isothermal potentiostatic cold start and observed that water freezes in the cathode electrode, microporous layer, and the GDL. Yana et al. [17] investigated the impact of sub-freezing temperatures on components and observed delamination of the catalyst layer during cold start. Mukundan et al. examined the fuel cell performance at subfreezing temperature and studied the

influence of carbon paper and carbon cloth GDLs [18]. Wang [19] presented theoretical analyses of PEFC cold start operation. Wang [19] identified different stages during cold start. Mao and Wang [20] and Meng [21] proposed multi-dimension cold-start models and examined the distributions of ice within the PEFC fuel cell assembly.

In view of the afore-mentioned approaches to cold start, theoretical analysis is highly desirable, particularly to identify and evaluate the key parameters governing the PEFC cold start operation. This paper develops a detailed analysis of cold start mechanisms via the pseudo 1D analysis of solid water variations along with the related overpotential change, which are critical to the fundamental understanding of fuel cell cold-start operation.

MODELING APPROACH

Figure 1 schematically shows the components of a PEFC and detail of cathode electrode. A PEFC consists of many components that are essential for its proper functioning including: bipolar plate, gas diffusion layer (GDL), catalyst layer (CL), and proton conducting membrane. The geometrical and physical parameters of these components are summarized in Table 1. At the electrochemical reaction surface in the cathode CL, oxygen reacts with protons and electrons from the hydrogen dissociation in the anode (see Fig. 1). Water and heat are byproducts of this reaction.

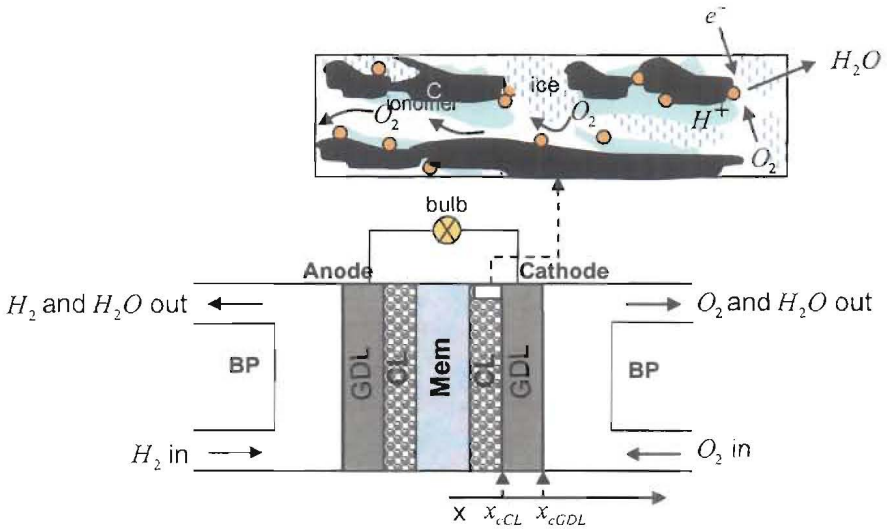

Fig. 1. Schematics of a PEFC and cathode electrode during cold start.

In the subzero environment, the above oxygen reduction reaction (ORR) is still active and able to produce water. Water production under subfreezing conditions has been observed indirectly by several experiments [12,14] (which show current production) and directly by neutron imaging, (see Fig. 2.). The neutron imaging shows water density images during operation under sub-freezing conditions (-20 °C). Cell was initially operated at 80°C and the channels were purged dry before shut-down and cooling in an environmental chamber to -20°C. After the cell reached -20°C, fuel cell operation was initiated at a constant current density of 0.02 A/cm^2 and anode and cathode flow of dry H_2 and dry air at 100 cc/min. The left side is the average water content during the initial 260 seconds of operation, while the right side is the average water content during the

final 260 seconds of an approximately 20 minute isothermal operation, which clearly shows water/ice accumulation in the fuel cell. The OCV at -20°C was 0.96V and when a current of 0.02A/cm^2 was applied, the voltage initially started at 0.79V and decayed to 0V over a time of 1130 seconds. At subfreezing temperature, water freezing in the pores of the catalyst layer blocks the open pores required for reactant diffusion. To avoid cold start failure, the fuel cell needs to be heated by either external sources or self-heating, to at least $0\,^{\circ}C$ before ice in the catalyst layer causes severe reactant starvation.

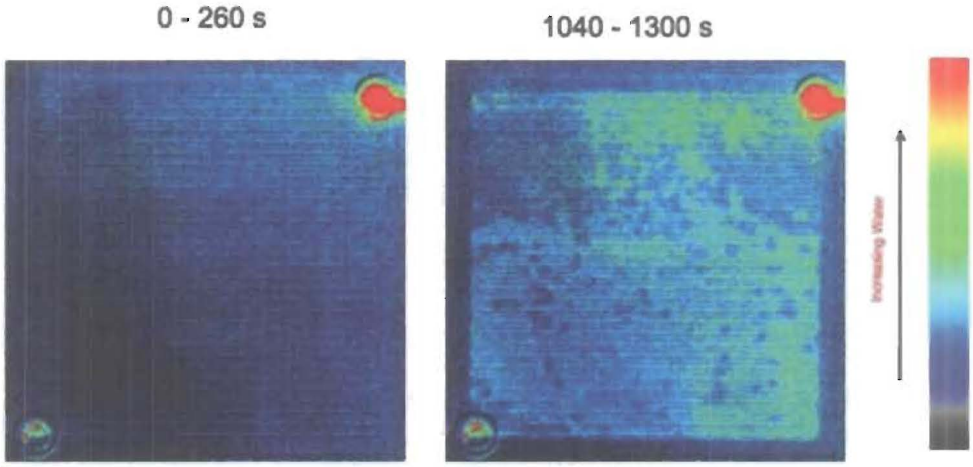

Fig. 2. Water density images in an operating PEFC by Neutron imaging at initial (left) and latter (right) stages of subfreezing operation (-20 °C). The left figure is the average water content during the initial 4.33 (260 sec) minutes of operation, while the right side is the final 4.33 (260 sec) minute average water content after approximately 20 minutes of a constant current (0.02 A/cm^2) operation.

For single-layer electrodes or homogenous electrodes, the spatial variation of the reaction rate across the catalyst layer is almost uniform at small $\hbar$ s ($\hbar = \dfrac{\Delta U}{2\dfrac{R_g T}{\alpha_c F}}$

where $\Delta U = \dfrac{I\delta}{\sigma_m^{eff}} = IR_\delta$) [22,23] (see Fig. 3), which is satisfied for most cold-start operation.

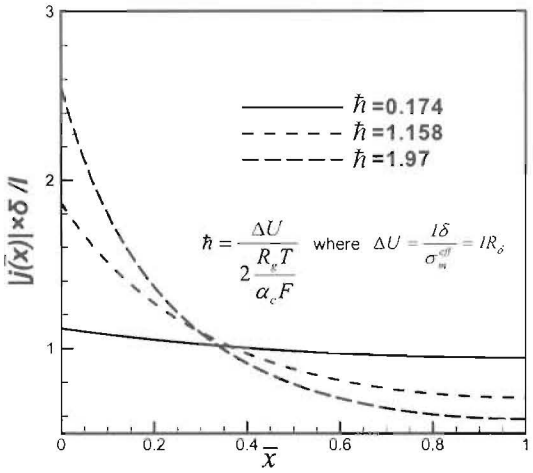

Fig. 3. Spatial variation of the reaction current densities at different $\hbar$ s [22,23].

However, when oxygen transport becomes a limiting factor due to solid water presence, the local reaction rate will vary in the electrode. At high *hs* (e.g. large current densities), even without solid water the reaction current will differ spatially. During cold start, the reaction rate in the cathode can be expressed as [19,22]:

$$j = -a_0 i_{0,c}^{ref}(1-s_{ice})^{\tau_a} \exp\left[-\frac{E_a}{R}\left(\frac{1}{T}-\frac{1}{353.15}\right)\right]\frac{C^{O2}}{C^{O2,ref}}\exp\left(-\frac{\alpha_c F}{RT}\cdot\eta\right) \quad (1)$$

In Eq. (1), α_c is the cathode transfer coefficient and its value depends on temperature [24]. The surface overpotential is defined as:

$$\eta = \Phi_s - \Phi_e - U_o \quad (2)$$

Φ_s and Φ_e are electronic and electrolyte phase potentials, respectively. Typically due to the high electronic conductivity, Φ_e remains constant in the cathode, while Φ_s usually varies spatially due to the ionic resistance. The equilibrium potential, U_o, is a function of temperature:

$$U_o = 1.23 - 0.9\times10^{-3}(T-298) \quad (3)$$

Eq. (1) directly shows that the reaction rate is a function of the local ice volume fraction as well as the local oxygen concentration. Both local ice volume fraction and oxygen concentration may vary spatially due to the local reaction and oxygen and water transport within the cathode. Therefore, the local reaction rate variation requires solving the coupled oxygen and water transport equations and electrochemical kinetics Eq. (1). A simplified assumption is to consider constant reaction rate in the electrode leading to uniform ice formation. Note that this assumption treats the catalyst layer as a number of separated small reactors in the through-plane direction. The reactors are operated at the

uniform reaction rate, allowing the surface overpotentials to vary according to the local oxygen content and ice volume fraction. This treatment greatly simplifies the model and enables the impact of ice on electrode performance to be evaluated through temporal and spatial variations of the surface overpotential. We refer to this analysis as the pseudo-1D analysis. The uniform local transfer current and oxygen consumption rate can be expressed as:

$$j = -\frac{I}{\delta_{CL}} \text{ and } S_{O2} = -\frac{I}{4F\delta_{CL}} \tag{4}$$

In addition, in the following analysis, we only consider the second stage of the cold start when ice starts to form in the cathode. Following the analysis of Ref. [19], the oxygen profile can be obtained by:

$$\frac{C^{O2}}{C_{cCL}^{O2}} = 1 - Da\frac{1-\bar{x}^2}{\varepsilon_{CL}^{\tau_d-\tau_{d,0}}[(1-s_{ice})]^{\tau_d}} \text{ where } \bar{x} = 1 - \frac{x_{cCL}-x}{\delta_{CL}} \tag{5}$$

where $\bar{x}$ is the dimensionless distance from the interface between the membrane and catalyst layer, and the dimensionless parameter, Da, is called the Damköhler number:

$$Da = \frac{I}{8F}\frac{\delta_{CL}}{C_{cCL}^{O2}D_K^{O2}\varepsilon_{CL}^{\tau_{d,0}}} = \frac{\text{Reaction rate}}{\text{Mass transport rate}} \tag{6}$$

Discussion on Da can be found in Ref. [19]. In addition, severe local oxygen starvation will first occur at $\bar{x}$=0 when C^{O2}=0, i.e.,

$$1 = Da\frac{1}{\varepsilon_{CL}^{\tau_d-\tau_{d,0}}[(1-s_{ice}^{starvation})]^{\tau_d}} \tag{7}$$

Assuming $\tau_d = \tau_{d,0}$, the above equation can be simplified as:

$$s_{ice}^{starvation} = 1 - \sqrt[\tau_d]{Da} \tag{8}$$

For $\tau_d = 2$ and $Da \sim 1.0 \times 10^{-4}$, $s_{ice}^{starvation}$ ~99%. Note that τ_d plays a critical role in determining the value of $s_{ice}^{starvation}$.

The oxygen profile in the catalyst layer of Eq. (5) can be substituted to Eq. (1), yielding [25]:

$$\eta(s_{ice},\bar{x}) = -\frac{RT}{\alpha_c F}\ln\left\{\frac{IC_{O2,ref}}{a_0 i_{0,c}^{ref}\exp\left[-\frac{E_a}{R}\left(\frac{1}{T_o}-\frac{1}{353.15}\right)\right]C_{cCL}^{O2}\delta_{CL}}\exp\left[\frac{E_a}{R}\left(\frac{1}{T}-\frac{1}{T_o}\right)\right]\right\} + \frac{RT}{\alpha_c F}\ln\left[(1-s_{ice})^{\tau_a}\left(1-Da\frac{1-\bar{x}^2}{\varepsilon_{CL}^{\tau_d-\tau_{d,0}}(1-s_{ice})^{\tau_d}}\right)\right] \quad (9)$$

Note that the impacts of ice are all included in the second term on the right while the first primarily accounts for the temperature-dependence of the exchange current density. The overpotential can further be written as [25]:

$$\eta(s_{ice},T,\bar{x}) = -\frac{RT}{\alpha_c F}\ln\left(\frac{IC^{O2,ref}}{a_0 i_{0,c}^{ref}\exp\left[-\frac{E_a}{R}\left(\frac{1}{T_o}-\frac{1}{353.15}\right)\right]C_{cCL}^{O2}\delta_{CL}}\right) - \frac{TE_a}{\alpha_c F}\left(\frac{1}{T}-\frac{1}{T_o}\right) + \frac{RT\tau_a}{\alpha_c F}\ln(1-s_{ice}) + \frac{RT}{\alpha_c F}\ln\left(1-Da\frac{1-\bar{x}^2}{\varepsilon_{CL}^{\tau_d-\tau_{d,0}}(1-s_{ice})^{\tau_d}}\right) = \eta_o + \Delta\eta_T + \Delta\eta_{c,1} + \Delta\eta_{c,2} \quad (10)$$

where

$$\eta_o = -\frac{RT}{\alpha_c F}\ln\left(\frac{IC^{O2,ref}}{a_0 i_{0,c}^{ref}\exp\left[-\frac{E_a}{R}\left(\frac{1}{T_o}-\frac{1}{353.15}\right)\right]C_{cCL}^{O2}\delta_{CL}}\right),\ \Delta\eta_T = -\frac{TE_a}{\alpha_c F}\left(\frac{1}{T}-\frac{1}{T_o}\right), \quad (11)$$

$$\Delta\eta_{c,1} = \frac{RT\tau_a}{\alpha_c F}\ln(1-s_{ice}) \text{ and } \Delta\eta_{c,2} = \frac{RT}{\alpha_c F}\ln\left(1-Da\frac{1-\bar{x}^2}{\varepsilon_{CL}^{\tau_d-\tau_{d,0}}(1-s_{ice})^{\tau_d}}\right)$$

RESULTS AND DISCUSSIONS

Table 1 Geometrical, physical and operating parameters	
Components	**Value**
Catalyst layer/GDL/BP thickness, $\delta_{CL}/\delta_{GDL}/\delta_{BP}$	0.01/0.2/1.0 mm
Porosity of GDLs/catalyst layers, $\varepsilon_{GDL}/\varepsilon_{CL}$	0.6/0.5
Volume fraction of ionomer in catalyst layers, ε_m	0.2
Activation energy for oxygen reduction reaction, E_a	73269 J/mol
Thermal conductivity of catalyst layer/GDL/BP,	0.3-3.0/0.28-3.0/20 W/m K
Density of ice/dry membrane, ρ_{ice}/ρ_m	917/1980 kg/m^3
O_2 diffusivity in cathode gas at standard condition, $D_{M,0}^{O2}$	3.24×10^{-5} m^2/s

Figure 4 shows the profiles of dimensionless oxygen concentration within the cathode catalyst layer. The oxygen concentration decreases when approaching the membrane due to the oxygen reduction reaction. The oxygen concentration variation is small in most cases, even at s_{ice} =98%, about 5% drop is indicated (using $\tau_d = 1.5$). However, the oxygen profile is sensitive to the tortuosity of the catalyst layer. Mukherjee et al. [26] estimated the tortuosity from reconstructed CL microstructures between 2.5 and 3.0. At CL tortuosity, $\tau_d = 2.5$, a considerable drop of oxygen concentration is present at s_{ice} =96%. As the oxygen concentration affects the mass transport polarization, the associated cell voltage loss becomes important only at high s_{ice} .

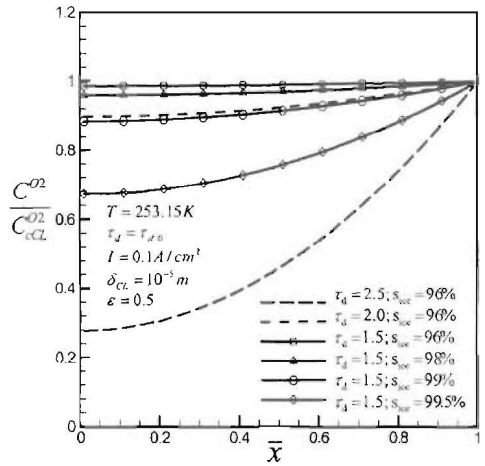

Fig. 4. Oxygen profiles in the cathode catalyst layer at different δ_{CL} s and ε_{CL} s at ice volume fraction of 0.98.

Figure 5 displays the profiles of the sum of the two overpotential variations related to solid water, $\Delta\eta_{c,1} + \Delta\eta_{c,2}$, across the cathode catalyst layer for different ice volume fractions. Among the two components in the plotted overpotential variation, only the second overpotential variation is dependent on location while the first one is solely a function of the local ice volume fraction. Consistent with the previous figure 4, the local oxygen transport polarization starts to become important at the high ice volume fraction, i.e. s_{ice} =99.7% in Figure 8. Even at s_{ice} =99%, the variation is still small and not evident. Further, the potential drop with s_{ice} primarily results from the first term in most range of

the cold-start, i.e. the mechanism of the ice coverage over the active reaction surface, which has been extensively discussed in Ref. [19].

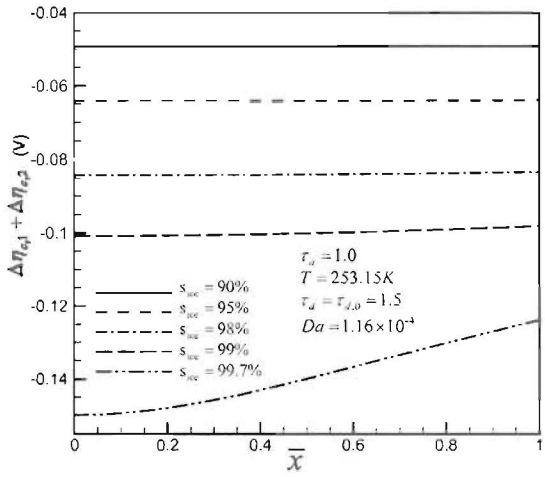

Figure 5. Profiles of $\Delta\eta_{c,1}+\Delta\eta_{c,2}$ across the cathode catalyst layer for different ice volume fractions.

Figure 6 compares the magnitudes of $\Delta\eta_T^{\max}$ and $\Delta\eta_{c,1}$. $\Delta\eta_{c,1}$ characterizes the impact of the ice coverage over the electrochemical reaction surface, and increases in magnitude quickly with s_{ice} as shown in Figure 6. Note that the ice coverage just temporarily blocks the oxygen access to the active reaction site, while the disabled interface, still accessible to electrons and protons, is generally able to recover after the solid water is removed. The figure shows that temperature has little impact on the value of $\Delta\eta_{c,1}$, instead the influence of the coefficient τ_α is evident. Further, the magnitudes of $\Delta\eta_T^{\max}$ are also indicated in Figure 6. Two values of the activation energy are considered [24]. Note that these values are according to different Tafel slopes with the higher value 73.3 KJ/mol corresponding to -60 mV/decade or low-current-density region while the other to -120 mV/decade or high-current-density region. The values of $\Delta\eta_T^{\max}$ plotted in the figure exclude the temperature-difference of the Tafel slope. Therefore the value primarily gives the magnitude of the overpotential change due to the temperature-dependence of exchange current density. From this figure, it can be seen that $\Delta\eta_{c,1}$ is comparable with $\Delta\eta_T$ at low and intermediate ice volume fraction regions, while $\Delta\eta_{c,1}$ dominates at the high fraction of s_{ice}. At s_{ice}>95%, the adverse impact of the solid water will lead to a fast drop of the cell voltage that has been observed in most studies [19, 21].

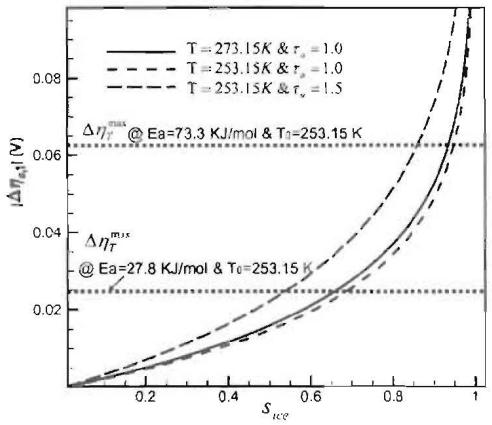

Figure 6. Comparison of the magnitudes of $\Delta\eta_T^{\max}$ and $\Delta\eta_{c,l}$.

CONCLUSIONS

This paper presents a theoretical study on the electrochemical and transport phenomena in the cathode catalyst layer of fuel cells for cold-start operation. Pseudo-1D analysis was developed and spatial variations of the oxygen concentration and overpotential were investigated. Oxygen transport limitation was found to occur at high ice volume fraction regions, especially in CL with high tortuosities. In addition, we decoupled the impacts from the temperature variation, ice coverage over the electrochemical reaction surface, and oxygen transport limitation during the cold-start and compared their magnitudes.

Acknowledgments

Partial support of this work by the UC Irvine Academic Senate Council on Research, Computing and Library Resources (CORCLR) is gratefully acknowledged.

References

[1]. C. Y. Wang, Chemical Reviews, 104, 2004, 4727.
[2]. Y. Wang and C.Y. Wang, Electrochimica Acta, 50, 2005, 1307.
[3]. R. Madhusudana Rao and R. Rengaswamy, Chemical Engineering Science, 61, 2006, 7393-7409.
[4]. Y. Wang and C.Y. Wang, Electrochimica Acta, 51, 2006, 3924.
[5]. Y. Wang and C. Y. Wang, J. Electrochem. Soc., 154, 2007, B636-643.
[6]. Hu, G. & Fan, J., J. Power Sources, 165, 2007, 171-184.
[7]. A.A. Shah, G.-S. Kim, P.C. Sui and D. Harvey, J. Power Sources, 163, 2007, 793-806.
[8]. Meng, H., J. Power Sources, 171 (2), 2007, 738-746.
[9]. Chang, S.-M., Chu, H.-S., J. Power Sources, 172 (2), 2007, 790-798 .
[10]. A.A. Shah, P.C. Sui, G.-S. Kim and S. Ye, J. Power Sources, 166, 2007, 1-21.
[11]. Y. Shan, S-Y Choe and S-H Choi, J. Power Sources, 165, 2007, 196-209.

[12]. Y. Hishinuma, T. Chikahisa, F. Kagami, and T. Ogawa, JSME Int. J., Ser. B, 47, 235 (2004).
[13]. M. S. Wilson, J. A. Valerio, S. Gottesfeld, Electrochim. Acta, 40, 1995, 355.
[14]. R. C. McDonald, C. K. Mittelsteadt, and E. L. Thompson, Fuel Cells, 4, 2004, 208.
[15]. E. Cho, J. J. Ko, H. Y. Ha, S. A. Hong, K. Y. Lee, T. W. Lim, and I. H. Oh, J. Electrochem. Soc., 151, 2004, A661.
[16]. M. Oszcipok, D. Riemann, U. Kronenwett, M. Kreideweis, and M. Zedda, J. Power Sources, 145, 2005, 407.
[17]. Q. Yana, H. Toghianib, Y-W. Leea, K. Liangb and H. Causey, J. Power Sources, 160, 2006, 1242.
[18]. R. Mukundan, Y. S. Kim, T. Rockward , J. R. Davey, B. S. Pivovar, D. S. Hussey, D. L. Jacobson, M. Arif, and R. L. Borup, ECS Transactions, 11, 2007, 543-552.
[19]. Y. Wang, J. Electrochem. Soc., 154, 2007, B1041-B1048.
[20]. L. Mao and C.Y. Wang, J. Electrochem. Soc. 154, 2007, B341.
[21]. H. Meng, Int. J. Hydrogen Energy, 33, 2008, 5738-5747.
[22]. Y. Wang and Xuhui Feng, J. Electrochem. Soc., 155(12), 2008, B1289-B1295.
[23]. Y. Wang and Xuhui Feng, J. Electrochem. Soc., 156(3) (2009) B403-B409.
[24]. Parthasarathy, S. Srinivasan, and A. J. Appleby, J. Electrochem. Soc., 139, 1992, 2530
[25]. Y. Wang, P. P. Mukherjee, J. Mishler, J. Chen, R. Mukundan, and R. L. Borup, J. Electrochem. Soc., submit.
[26]. P. P. Mukherjee and C. Y. Wang, J. Electrochem. Soc., 153, 2006, A840-849.